Interannual Variability of Patterns of Atmospheric Mass Distribution

KEVIN E. TRENBERTH, DAVID P. STEPANIAK, AND LESLEY SMITH

National Center for Atmospheric Research, Boulder, Colorado*

(Manuscript received 13 February 2004, in final form 28 July 2004)

ABSTRACT

Using the 40-yr European Centre for Medium-Range Weather Forecasts (ECMWF) Re-Analysis (ERA-40) for 1958 to 2001, adjusted for bias over the southern oceans prior to 1979, an analysis is made of global patterns of monthly mean anomalies of atmospheric mass, which is approximately conserved globally. It differs from previous analyses of atmospheric circulation by effectively area weighting surface or sea level pressure that diminishes the role of high latitudes. To examine whether global patterns of behavior exist requires analysis of all seasons together (as opposite seasons occur in each hemisphere). Empirical orthogonal function (EOF) analysis, *R*-mode varimax-rotated EOF analysis, and cyclostationary EOF (CSEOF) analysis tools are used to explore patterns and variability on interannual and longer time scales. Clarification is given of varimax terminology and procedures that have been previously misinterpreted. The dominant global monthly variability overall is associated with the Southern Hemisphere annular mode (SAM), which is active in all months of the year. However, it is not very coherent from month to month and exhibits a great deal of natural unforced variability. The third most important pattern is the Northern Hemisphere annular mode (NAM) and associated North Atlantic Oscillation (NAO), which is the equivalent Northern Hemisphere expression. Neither of these is really a global mode, although they covary on long time scales in association with tropical or external forcing. For monthly data, the second mode is coherent with Niño-3.4 sea surface temperatures and thus corresponds to El Niño–Southern Oscillation (ENSO), which is truly global in extent. It exhibits more coherent evolution with time and projects strongest onto the interannual variability, where it stands out by far as the dominant mode in the CSEOF analysis. The CSEOF analysis extracts the patterns phase locked with annual cycle and reveals their evolution throughout the year. Standard EOF and varimax analyses are not able to evolve with time of year unless the analysis is stratified by season. Varimax analysis is able to extract the SAM, NAM, and ENSO modes very well, however.

1. Introduction

The global mass of the atmosphere is approximately conserved. More precisely, the global mass of dry air changes slowly in conjunction with changes in composition of the atmosphere. Overall, Trenberth and Smith (2005) estimate that the global dry air mass is constant to within 0.01-hPa-equivalent global surface pressure. Trenberth and Smith (2005) further examined several global reanalyses to see how well the global dry air mass constraint is met and derived new values for the total mass of the atmosphere based upon the 40-yr European Centre for Medium Range Weather Forecasts (ECMWF) Re-Analysis (ERA-40). They documented the annual cycle of total mass and water vapor and found that the dry air mass is constant in the ERA-40 reanalyses to within a standard deviation of 0.065 hPa for monthly mean fields after 1979. Prior to 1979, and especially prior to 1973 when satellite data are not available, the constraint is not close to being met and problems are identified, especially over the southern oceans.

Many previous analyses exist of sea level pressure fields using techniques such as empirical orthogonal functions (EOFs) and correlation analysis to determine teleconnection patterns. For instance, EOF analysis of Northern Hemisphere (NH) sea level pressures north of 20°N for 1925–77 by Trenberth and Paolino (1981) found that the dominant pattern in all seasons is what is now called the Northern Hemisphere annular mode

* The National Center for Atmospheric Research is sponsored by the National Science Foundation.

Corresponding author address: Dr. Kevin E. Trenberth, National Center for Atmospheric Research, P.O. Box 3000, Boulder, CO 80307.
E-mail: trenbert@ucar.edu

(NAM). Moreover, they related it to the North Atlantic Oscillation (NAO). More generally, results from all of the previous analyses vary somewhat and depend on details of how the analysis was carried out, such as the domain used, what grid was used, and whether values were weighted in some way (e.g., Barnston and Livezey 1987). Most commonly, gridded latitude–longitude analyses have been used and a $\cos\phi$ weighting has been applied to the computed variances and covariances to take account of the convergence of meridians with latitude, effectively area weighting the covariances. In these cases, the quantity analyzed has indeed been the sea level pressure, which has the advantage that it is not sensitive to modest changes in elevation of the measurement (i.e., station moves). The disadvantages are that sea level pressure effectively adds a temperature-dependent artificial mass of atmosphere to replace the topography and is not area weighted and, hence, is less directly related to the true mass distribution.

Therefore, analyzing the surface pressure appears to have major benefits relative to sea level pressure by eliminating the necessity of extrapolating below ground over land. Several estimates of the global mean surface pressure, p_s, differ because of topography changes in the models used in the analyses (Trenberth and Smith 2005). Also, as direct use of p_s values includes large gradients near mountains, it is desirable to use departures from the long-term monthly means for analysis of atmospheric variations.

Further, there is considerable merit in analyzing a quantity that has a global constraint of being conserved, namely mass. Mass is proportional to surface pressure (Trenberth and Smith 2005) but incorporates area weighting. Hence, relative to sea level or surface pressure, an analysis of mass effectively weights each value by $\cos\phi$, or the variance by $\cos^2\phi$, and thus it diminishes the influence of the high latitudes on results. Only for mass is high pressure in one region fully compensated for by low pressure elsewhere. A good example is the occurrence of major blocking episodes in which there is a buildup of high pressure over a region, but the compensating low pressure may occur in the other hemisphere (e.g., Trenberth 1986; Carrera and Gyakum 2003). This argument also suggests that the domain should be global and hence there is no reason to favor a particular season: winter in one hemisphere accompanies summer in the other.

The goal of this study is to perform an analysis of atmospheric mass in a systematic way and determine whether the dominant patterns that emerge relate to well-established modes or patterns of atmospheric variability such as El Niño–Southern Oscillation (ENSO), the NAO, and so on. We begin with a conventional EOF analysis of appropriately area-weighted monthly anomalies of p_s. Hence, water vapor contributions are included, although their contribution to the variability is quite small (Trenberth and Smith 2005). The period analyzed is 1958 to 2001 from ERA-40, with an adjustment made over the southern oceans to homogenize the anomalies somewhat. Nevertheless, this is a finite period and because EOF analysis attempts to account for the maximum variance explained, modes of behavior that otherwise might be sifted out with a much longer dataset are apt to become intermingled with one another. Accordingly, we also perform a varimax rotation of the EOFs (VEOF analysis) to simplify the structure.

Even though long-term monthly means are removed, the variance is still not stationary as it contains a distinctive annual cycle, especially locally. Variability is much greater in the winter hemisphere. Accordingly, the statistics have a distinctive annual cycle that should be recognized in the analysis; rather than simply analyze the seasons separately, we employ a cyclostationary EOF (CSEOF) analysis (Kim and North 1997). This provides a rather different perspective on interannual variability, and perhaps one that may be of value in other applications.

Section 2 describes the dataset, the modifications made to it, and the methods of analysis, including clarification of terminology in use in atmospheric sciences. Section 3 presents the results of conventional EOF analyses, varimax EOF analyses, and CSEOF analysis, and further discusses the results in the context of patterns of known modes of behavior of the atmosphere. Section 4 presents the conclusions.

2. Datasets and methods

a. Data

The main data employed in this analysis are surface pressure analyses from ERA-40, most often truncated to T63 resolution on a Gaussian grid with resolution of 1.875°, or T42 (2.8°). The analysis is of monthly anomalies; however, to reduce noise associated with synoptic weather systems crossing from one region to another at the beginning and end of months, the main analysis is of anomalies smoothed with a ¼(1–2–1) binomial filter that removes two-month fluctuations and hence cuts the number of independent values in half. Figure 1 shows the percentage variance retained in this process and highlights the exceptionally noisy nature of monthly means in the extratropics. In the Tropics some of this noise is from fluctuations with about monthly time scales, such as the Madden–Julian oscillation, but elsewhere most of this is indeed weather noise.

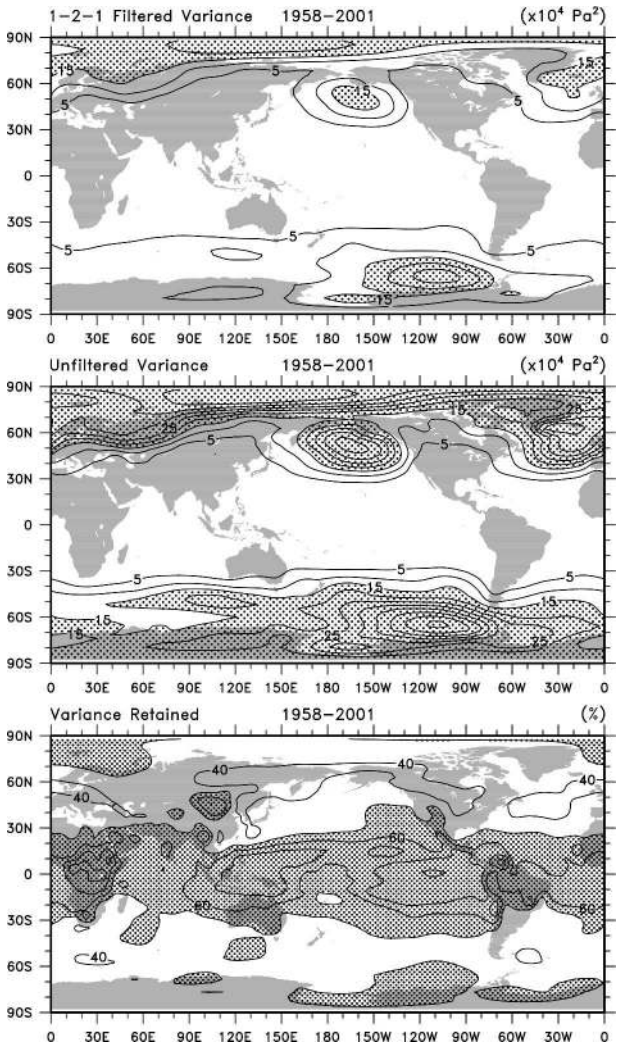

FIG. 1. For the surface pressure monthly anomalies on a T42 grid for 1958–2001, shown are (middle) the unfiltered monthly variance, units 10^4 hPa^2; (top) the 1–2–1-smoothed variance; and (bottom) the percent variance retained.

An evaluation of these data (Trenberth and Smith 2005), in the context of the conservation of mass of the atmosphere, found spurious trends in both the mass of dry air and atmospheric moisture arising from changes in the observing system, especially prior to 1979 when reliable satellite data became available for global analyses. Spurious fluctuations in global mean surface pressure of order 0.6 hPa occur before 1979 and primarily arise from low-quality analyses over the southern oceans. Surface pressures are generally higher around Antarctica and contribute to global mean values of order 0.3 hPa higher before 1973 in ERA-40. Locally, around Antarctica, errors were shown to be of order 5 hPa. The Vertical Temperature Profile Radiometer (VTPR) data, available from 1973 to 1978, improve both the mean state and cut down on spurious variability, but are not as good as the post-1979 data in this regard. It also leads to water vapor column values that are too high in the subtropics. Water vapor mean annual cycle variations are found to contribute to global mean surface pressure variations of 0.3 hPa. In general, water vapor contributions to total mass anomalies are much smaller and can be neglected for current purposes. Spurious trends in sea level pressure from analyses, especially the National Centers for Environmental Prediction–National Center for Atmospheric Research (NCEP−NCAR) reanalyses have also been identified by Marshall (2003).

However, the spurious variations in mass prior to 1979 are regarded as a potential problem for exploring variability because they artificially inflate the variance, unless corrected. Accordingly, based on the mean errors documented in Trenberth and Smith (2005), some adjustments were made to the surface pressure anomaly time series in a region bounded by 56°S and the Antarctic coast. In this region for post-1979, and other regions as well, the mean annual cycle from 1979 to 2001 is used to determine the monthly anomalies. A core region from 56°S to within 2.25° latitude of the coast was established with a mask where full adjustments are made, whereby the anomalies prior to 1979 were computed relative to the mean for 1958–78. For two grid points immediately north and south of the core region, a merge is devised such that the weights are two-thirds and one-third, with the two-thirds weight closest to the core (inner) region. Some minor smoothing to the mask was made in the vicinity of the Antarctic Peninsula. Accordingly, decadal variability across 1978–79 is suppressed in this region. (The adjusted surface pressure anomalies are available from NCAR at http://www.cgd.ucar.edu/cas/catalog/ecmwf/era40.)

b. EOF analysis

The first analysis is a standard EOF analysis (see Richman 1986 for a review) of monthly anomalies of mass, where the units are kilograms. In our terminology, EOFs are eigenfunctions of the covariance matrix. The loading vectors depict normalized EOF spatial patterns that are then converted into more familiar equivalent surface pressure patterns. Along with each pattern is a principal component (PC) time series and an eigenvalue that can be normalized by the total variance to provide the fraction of variance accounted for by each EOF. Usually the EOFs are ordered by the amount of variance accounted for. This kind of analysis results in orthogonal patterns and time series (at zero lag) and hence is a very efficient representation of the variance. The results may produce patterns that are physical

modes of the climate system, but in general this is unlikely. Results typically depend on the variable being analyzed, the domain used, whether the data are normalized (so that the eigen analysis is of the correlation rather than covariance matrix), time scales and filtering, and so on. Disadvantages discussed by Richman (1986) are not necessarily accepted by Jolliffe (1987). In particular, as the method attempts to account for the most variance, it tends to result in EOF patterns that are global in extent. For instance, Rossby wave teleconnections are known to result from certain kinds of disturbances but may be somewhat local and confined to one hemisphere. But EOFs will populate the domain with patterns that happen to be correlated for this particular sample; yet, unless there is a physical relationship, the apparent links will change as data are added, and the results will not be robust.

c. Varimax EOF analysis

Accordingly, we decided to also perform a varimax rotation, a now widely used algorithm whose characteristics and rationale are described by Horel (1981). It is claimed to be more robust to temporal and spatial domains (Richman 1986), but results depend a great deal on the number of eigenvectors chosen for rotation. Rotation conserves the total variance of the eigenvectors selected for rotation but redistributes it at the expense that successive maximization of variance is lost (Jolliffe 1987). Performing a rotation with varimax retains orthogonality of either the spatial patterns or the time series, *but not both*. It also imposes a "simple structure" to the fields that tends to localize the main centers of action and maximize the regions of small weightings.

To be more specific and clarify the terminology, in EOF analysis, time series of a spatial array of gridded data $P(\mathbf{r}, t)$ are represented in terms of EOF loading vectors $V(\mathbf{r})$ and their principal component time series $T(t)$, where $\mathbf{r}$ is the vector depicting the spatial dimension

$$P(\mathbf{r}, t) = \sum_i V_i(\mathbf{r}) T_i(t), \tag{1}$$

so that V depicts the spatial patterns of the EOF and is an eigenvector of the analysis. The index i represents the number of EOFs, each associated with an eigenvalue λ_i. Commonly, only a few of the EOFs are retained for further analysis.

There is a symmetry in the separation of variables in space and time in (1) whereby we can readily switch time for space, or vice versa. In factor analysis (e.g., Davis 1986), the focus tends to be on either one or the other. In Q-mode factor analysis, attention is centered on the interpretation of the time variations (or in more general statistical terminology "inter-object relationships"). In this case with varimax, the orthogonality is retained in the principal component time series but not the patterns. The alternative is to focus on the spatial patterns, called R-mode factor analysis, where the "inter-variable relationships" are explored. In this case for varimax, the resulting spatial patterns are orthogonal but the time series are not.

In atmospheric sciences, it has frequently been claimed that the orthogonality in space is artificial and hence that constraint should be relaxed but that orthogonality in time is important. For instance the rotated principal component analysis (RPCA) of Horel (1981), Lanzante (1984), and Barnston and Livezey (1987) make this claim and seem to suggest that they are performing a Q-mode varimax analysis; yet closer examination eventually makes clear that they were, in fact, performing an R-mode analysis. A consequence is that there is widespread confusion over terminology and use of varimax in meteorology. Because the time series are correlated in R-mode varimax, the temporal variance locally is not uniquely partitioned among the patterns. However, it turns out that it is uniquely partitioned when summed over the entire spatial grid owing to the orthogonality of the patterns! Accordingly, it is still possible to uniquely assign the fraction of variance accounted for to VEOFs in spite of lack of orthogonality of the time series. However, this does have other consequences. In the commonly used R-mode varimax analysis, the operation of developing the simple structure is performed on the spatial patterns and, given the new VEOF patterns, the associated time series is computed by projecting the patterns onto the original data. However, if the resulting time series are then projected back onto the data to compute, for instance, a spatial correlation pattern, then the result has no direct relationship with the VEOF pattern because of the cross-correlation among time series. In contrast for standard EOFs, the correlation pattern can be derived directly from the EOF pattern and the zero lines remain fixed. Hence, there are at least two spatial structures associated with each VEOF. We will use the R-mode varimax analysis and illustrate some of these points.

d. Cyclostationary EOF analysis

Some of the potential problems with EOF analysis related to dependence on domain are removed through use of global data. However, the seasonal dependence of variability in each hemisphere demands recognition of the annual cycle of variance, even if the mean annual cycle is removed. This can be accomplished with cyclo-

stationary EOFs (Kim and North 1997). This technique assumes a periodic temporal evolution with a period, in our case, of the annual cycle. With some reasonable approximations Kim and North (1997) derive a computationally efficient way using Bloch functions to produce these CSEOFs. Several key characteristics are important for understanding the results. For monthly time series, the CSEOF procedure results in periodic loading vectors and hence one for each month of the year. These are the "nested" fluctuations with periods less than a year (intraannual in Kim and North's parlance). An EOF computation is performed with CSEOFs obtained as eigenfunctions of the cyclic covariance function resulting in the Bloch functions (EOF patterns) that are cyclic but which evolve with interannual variations (the outer modes of Kim and North), given by the principal component time series. Usually only the first few CSEOFs are of interest. The time series will include any harmonics of the annual cycle but, otherwise, the periods are longer than the nested period. An example application is given in Kim and Chung (2001).

In CSEOF analysis, a similar representation to that in standard EOF analysis (see above) is used:

$$P(\mathbf{r}, t) = \sum_i V_i(\mathbf{r}, t) T_i(t) , \qquad (2)$$

except that now the spatial patterns also have a cyclic time dependence such that $V(\mathbf{r}, t) = V(\mathbf{r}, t + d)$, where d is the period, in our case, of the annual cycle (=12 months). Note that $V(\mathbf{r}, t)$ and $T(t)$ are orthogonal.

We have experimented with the CSEOF technique on several datasets and worked closely with K.-Y. Kim, who kindly provided the initial software for producing these computations. Subsequently, we have modified the software to conform to the FORTRAN 90/95 standard as much as possible, invoked public domain alternatives for certain proprietary dependencies, and written a generalized interface. The interface, software, and documentation are available online (see http://www.cgd.ucar.edu/cas/software/list.html). Our experience leads us to note that the qualitative and quantitative characteristics of the ends of the output PC time series (say the first and last year of monthly mean data for example) depend on the temporal length of the input time series. This cannot be emphasized enough. The reason is that a localized window (approximately, a Morlet mother wavelet function implemented to render a localized Fourier transform within the "nested period") is applied to the data (K.-Y. Kim 2002, personal communication). At the end points of the input time series, only half of the window is being applied, no matter how one selects or preconditions the end portions of the data. Hence we find that it is best to ignore a segment of length equal to the nested period at the beginning and end of the output PC time series.

Usually, the CSEOF analysis is applied to data with the annual mean removed but, where the annual cycle is retained, it allows the analysis to pick out the mean annual cycle as the first, and usually by far dominant, mode. Then the time series depicts interannual fluctuations in amplitude of the mean annual cycle. Higher modes are then apt to be modes of variability that are phase locked to the annual cycle, such as ENSO, which has its maximum fluctuations in sea surface temperature (SST) in December (Trenberth et al. 1998). We have performed such an analysis that includes the annual cycle, and the first mode essentially reproduces the monthly mean departures from the annual mean. We will therefore focus on the CSEOF analysis of the anomaly time series after removing the mean annual cycle in the conventional way by subtracting the monthly means, but this still retains the annual cycle in variance.

The results of our analyses produce spatial structure maps of mass anomalies, which are not familiar to most of us, and therefore we translate these into equivalent surface pressure maps by dividing by the Gaussian weight (proportional to the area) and renormalizing. We also present some correlation maps and, alternatively, could regress the PC time series on surface pressure.

e. Circulation indices

We can then relate the patterns and time series to known modes or identified patterns of variability through both the correlation of the time series and through the spatial patterns. Barnston and Livezey (1987) provide a thorough overview of many of these modes and circulation indices. In particular, we compare these patterns and time series with ENSO indices of the Southern Oscillation index (SOI) (Trenberth 1984; see http://www.cgd.ucar.edu/cas/catalog/climind/soi.html) and Niño-3.4 SST (Trenberth and Stepaniak 2001; see http://www.cgd.ucar.edu/cas/catalog/climind/TNI_N34/index.html#Sec5) and the North Pacific index (NPI) of Trenberth and Hurrell (1994; see http://www.cgd.ucar.edu/~jhurrell/np.html#monthly), which is also an index of the Pacific decadal oscillation (PDO). See especially the discussion by Newman et al. (2003) and the NAO index (Hurrell 1995; http://www.cgd.ucar.edu/~jhurrell/nao.stat.other.html#monthly), NAM, and the Southern Hemisphere annular mode (SAM) of Thompson and Wallace (2000): NAM = AO (Arctic Oscillation) from NOAA's Climate Prediction Center (CPC; see http://www.cpc.ncep.noaa.gov/products/precip/CWlink/daily_ao_index/ao_index.html); SAM =

TABLE 1. Percentage variance (Var) explained by the first 10 EOFs for the 1–2–1 monthly mass anomalies. Also given is the standard error (SE). The last row gives the percentage variance associated with four rotated varimax EOFs (VEOF).

	EOF									
	1	2	3	4	5	6	7	8	9	10
Var	12.2	8.6	7.4	6.3	5.2	5.0	4.0	3.6	3.4	3.3
SE	0.75	0.53	0.45	0.39	0.32	0.31	0.24	0.22	0.21	0.20
VEOF	10.2	9.2	8.5	6.7						

AAO (Antarctic Oscillation) from CPC (see http://www.cpc.ncep.noaa.gov/products/precip/CWlink/daily_ao_index/aao/aao_index.html or more completely, http://www.jisao.washington.edu/data/aao/slp/).

3. Results

Although we have performed several experimental analyses with the raw monthly mass anomalies, it is apparent that they involve considerable noise arising from incompletely sampled weather systems that is considerably reduced by application of the 1–2–1 smoother. A map of the monthly mean variance of surface pressure at T42 resolution is given (Fig. 1) along with the result for the filtered data and the percentage variance retained. Over 70% of the variance is retained in much of the Tropics and subtropics except over the Indian Ocean where intraseasonal (Madden–Julian) oscillations on order of monthly periods are reduced in influence. In the extratropics, only roughly half the monthly variance is retained. Summed over the entire globe, the monthly mean mass variance is accounted for by the annual cycle (51.4%) and 48.6% by the monthly anomalies, of which 47.7% (or 23.1% of the total) is retained by the 1–2–1 filter. To illustrate interannual variability, we will also make use of an 11-point binomial filter (Trenberth 1984) that removes fluctuations less than 9 months but retains 24-month periods with 80% amplitude. For the mass field, such a filter retains >50% of the variance over about half of the Tropics but only 10% to 20% of the anomaly variance in the extratropics.

a. EOF analysis

A standard EOF analysis results in the same dominant patterns through the first six EOFs for both monthly and 1–2–1 smoothed results. Table 1 presents the percentage variance explained by the first 10 EOFs, and the first two EOFs and their time series are given in Fig. 2. The first six EOFs account for 44.7% of the variance. The estimated standard error of the eigenvalues (Table 1) suggests that the first four are distinct, the next two may be mixed, and numbers 7 through 10 are too close to be distinct from each other although they are distinct from the previous pair.

Although the analysis is of the mass field, we present the equivalent surface pressure fields, and only the first two EOFs are shown, as they illustrate the need to apply a rotation and simplify the structure. They are related to several common indices of circulation. The dominant pattern for EOF1 is that of the SAM (correlation of monthly anomalies is 0.55 for 1958–2001), but it also includes a clear El Niño signature throughout the Pacific (correlation with the Niño-3.4 SST index of –0.50). For EOF2 the correlations are with the NAO (0.31) and NAM (0.51), but also with ENSO (0.43) mixed in. These correlations vary with season; for example, the correlation for EOF2 with NAM is 0.60 for the northern winter half year, while it is higher (0.59) with ENSO in the summer half year.

b. Varimax EOF analysis

Because the EOF paradigm accounts for the most variance and thus selects patterns with global weightings, they are not likely to be physical modes in any sense, and thus we experimented with varimax rotation of various numbers of EOFs. The lack of sufficient separation of the eigenvalues means that it makes sense to consider rotating only 2, 3, 4, 6, or 10 patterns, and there is no convergence as higher numbers are included. Instead, as more and more EOFs are included, the patterns become more localized. We have chosen to present results for rotation of the first four VEOFs totaling 34.6% of the variance (Fig. 3); see Table 1 for the percentage variance accounted for by each. The associated principal component monthly time series, along with a low-pass filter applied to highlight interannual variations, is given in Fig. 4.

As noted in section 2, the time series are not orthogonal although, because the cross correlations are not high, they can be treated as somewhat independent. VEOF1 is correlated with VEOF2 at 0.19, VEOF3 at 0.16, and VEOF4 at 0.01; these are the highest values except VEOF4 has maximum correlation with VEOF2 at 0.12. Hence the common variance is less than 4% in all cases. The time series also exhibit varying degrees of

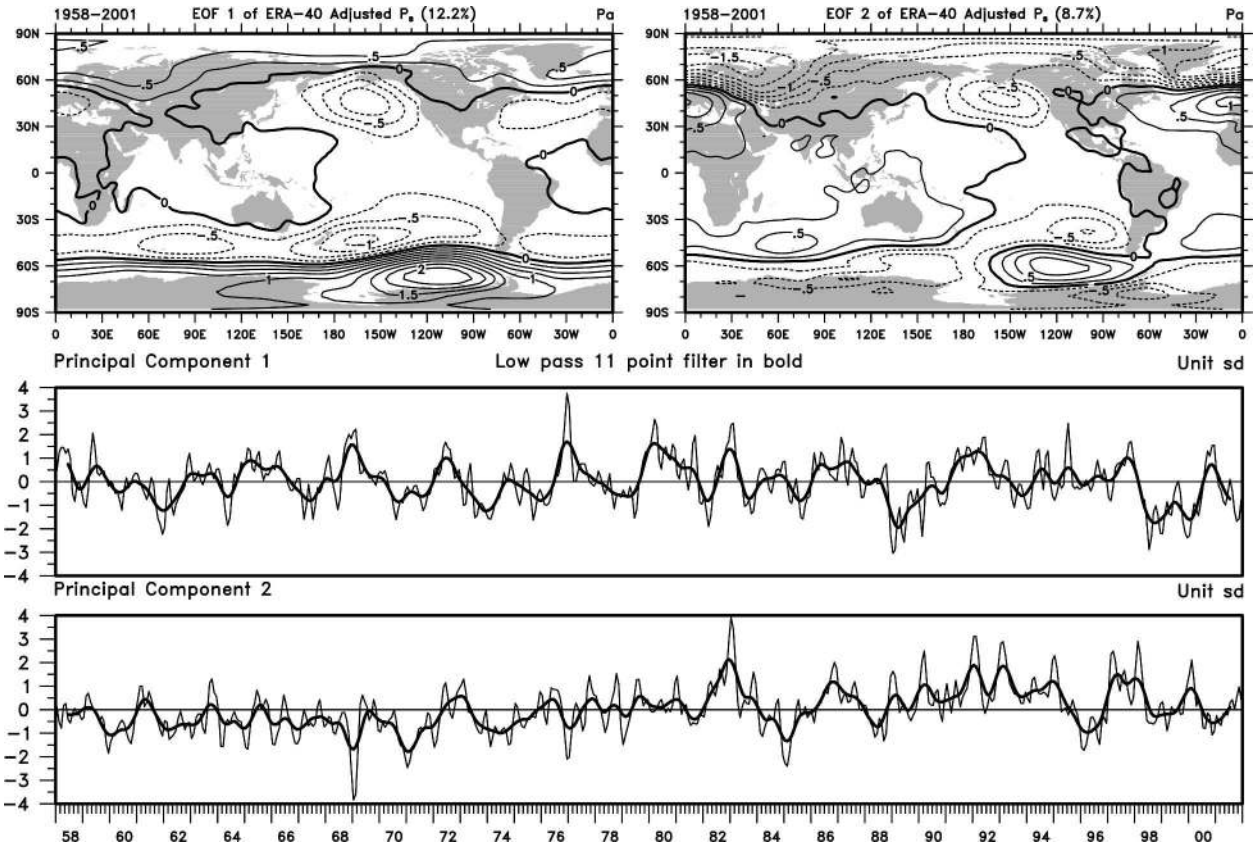

FIG. 2. The first two EOF patterns from the global mass analysis using 1–2–1-filtered monthly anomalies expressed as surface pressures. Negative values are dashed. Also shown are the PC time series along with a low-pass (11 term) filter that reveals the interannual variability.

autocorrelation. The lag-1 autocorrelations are all quite high (Table 2), but at lag 4 months these all drop substantially except for VEOF2 (Table 2); it is not until 9 months that the autocorrelation for VEOF2 drops below 0.2. Hence persistence and lower-frequency fluctuations are mainly evident only in VEOF2, as can be seen from the low-pass filter.

Because the analysis is based upon monthly anomalies, it depends upon the distribution of variance throughout the year. For these four VEOFs, most total variance (3.25%) comes from January, closely followed by February, July, December, June, and August. The lowest is April (2.43%) and October and November are also quite low (2.6%). This is especially evident in VEOF1, while VEOF2 has maximum variance in the southern winter, VEOF3 peaks in February and March, and VEOF4 peaks in January, September, and February, with minima in April–May. Surprisingly, none of these patterns are characterized simply as northern or southern winter patterns.

Correlations of the VEOFs with established patterns of variability from 1958 to 2001(Table 3) are based on 264 independent values for which the 5% two-tailed significance level is 0.12. For 1979–2001, it is 0.17. Note that there has been a substantial increase in VEOF1 correlation with SAM (0.68) compared with EOF1 (0.55) while it is no longer significantly related to El Niño indices. In fact, the VEOFs can be readily identified primarily with one of the predominant known modes of variability. VEOF1 is SAM, and VEOF 2 is primarily El Niño (through either the SOI or Niño-3.4 index) and also relates to NPI, which is closely related to the PDO. VEOF3 is primarily NAM, which is closely related to NAO, and also has a link with NPI. VEOF4 is more closely identified with NPI.

When the correlations are computed over the shorter interval from 1979 to 2001, the values are fairly stable except for those with SAM, which is much higher at 0.83 for the shorter period. This no doubt relates to the various sources of data for computing SAM, and in particular, if the NCAR–NCEP reanalyses are used, then there are large spurious trends in SAM, especially in the winter (Marshall 2003). As we noted earlier, it was necessary to correct the ERA-40 reanalyses in the

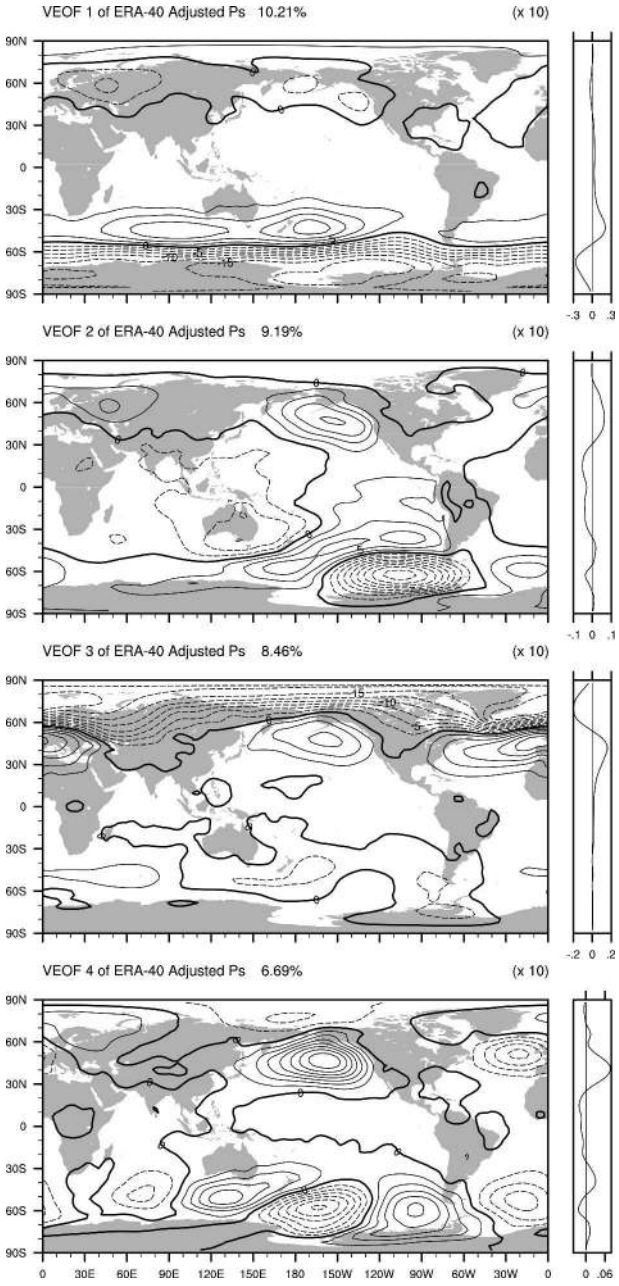

FIG. 3. The first four VEOF patterns for 1958–2001 monthly mass anomalies, smoothed 1–2–1 and expressed as equivalent surface pressure anomalies. Negative values are dashed. The contour interval is 0.25, and contours are multiplied by 10. The zonal integral is given at right to indicate mass redistribution.

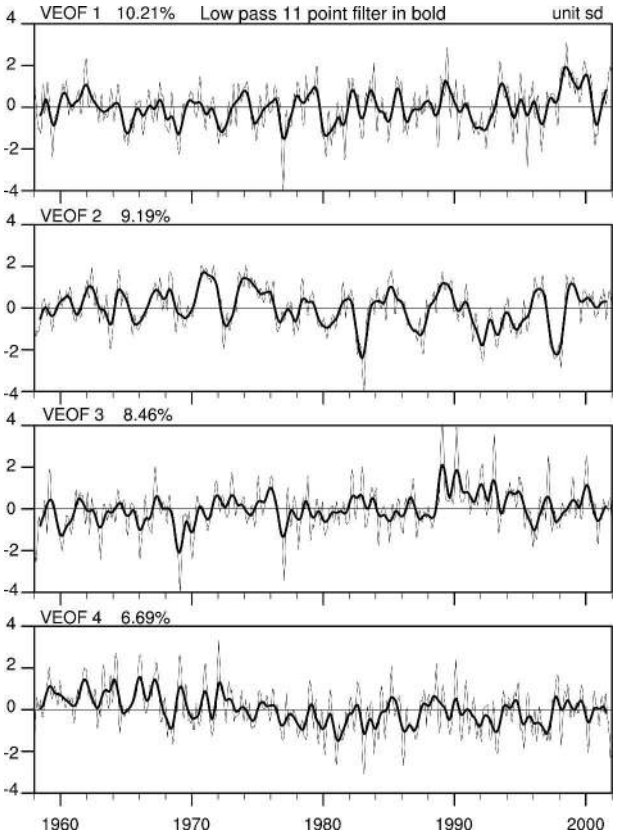

FIG. 4. The PC time series of the first four VEOFs along with the 11-term low-pass filter (heavy curve) for 1958–2001.

southern oceans region before we performed the current analysis. Therefore it is expected that the true correlation is probably greater than 80% and the VEOF1 time series is probably a more reliable depiction of SAM variations. When the time series are filtered (heavy curves in Fig. 4), correlations increase for VEOF1 and SAM (0.71) and VEOF 3 with NAM (0.97) and NAO (0.72), but while VEOF2 correlations increase with SOI (0.90), they go down somewhat for Niño-3.4.

The spatial patterns (Fig. 3) can also be interpreted through correlations with the time series (Fig. 5) although these are contaminated by the lack of orthogonality (see section 2). At the right side of the VEOF patterns (Fig. 3), the zonal integral profile is plotted, which therefore relates to the meridional distribution of mass associated with each pattern.

For VEOF1, Fig. 3 reveals the seesaw of mass across about 50°S associated with the SAM. It therefore reveals the strong changes in the westerlies throughout

TABLE 2. Autocorrelations at lags in months for the varimax EOFs.

	VEOF			
	1	2	3	4
Lag 1	0.78	0.89	0.79	0.77
Lag 4	0.20	0.50	0.10	0.09

TABLE 3. Correlations (as percent) of the VEOFs with climate indices. These are all for monthly values from 1958 to 2001. Values in bold are all highly statistically significant.

	Index					
VEOF	NAM	NAO	SAM	NPI	Niño-3.4	SOI
1	10	−1	**68**	3	−15	11
2	8	0	8	38	**−77**	**72**
3	**83**	**51**	14	31	−13	6
4	11	1	−6	**62**	−2	10

the Southern Hemisphere from 40° to 65°S. The correlation pattern (Fig. 5) reveals that the entire Pacific Ocean is coherent with the mass from 20° to 50°S, and other parts of the Tropics are also involved. Although this pattern does not map onto the Southern Oscillation (SO), its influence in the South Pacific (e.g., at Tahiti) would interfere somewhat with the simple Tahiti–Darwin SO index.

VEOF2, especially when viewed as a correlation pattern (Fig. 5), clearly incorporates the SO (e.g., see Trenberth and Caron 2000) throughout the Tropics and subtropics. Hence, associated with El Niño are higher pressures over Australia across Africa to Northeast Brazil and lower pressures over the central Pacific. The associated deeper Aleutian low and pattern over Asia is a strong northern winter signature, while the strong wave train (as indicated by the sequence of high and low centers) from Australia across the South Pacific (Fig. 3) is more evident in southern winter and spring (June through November). Note that the meridional distribution of mass associated with this mode is truly global. The time series depicts the well-known historical El Niño events and reveals the biggest El Niño event as 1982–83 by this measure, followed by 1997–98, with the general trend toward lower values after the climate shift in 1976 also seen.

VEOF3 is entirely a Northern Hemisphere mode and signifies low pressures over the Arctic accompanied by higher pressures over the Pacific and especially the Atlantic. It maps onto the NAM and, in the Atlantic sector, the NAO. The time series is strong in all months except April and tends to feature strong peaks, most often in northern winter. It features mostly below-normal values in the 1960s, especially 1969, and sharply above normal values in the late 1980s and early 1990s, as is also known to be the case for the NAO for December through March (Hurrell et al. 2003).

VEOF4 features the North Pacific region, and hence the links to the NP index, but also features a strong remarkably coherent wave train across the Southern Hemisphere that extends from the southern Indian Ocean to the South Atlantic.

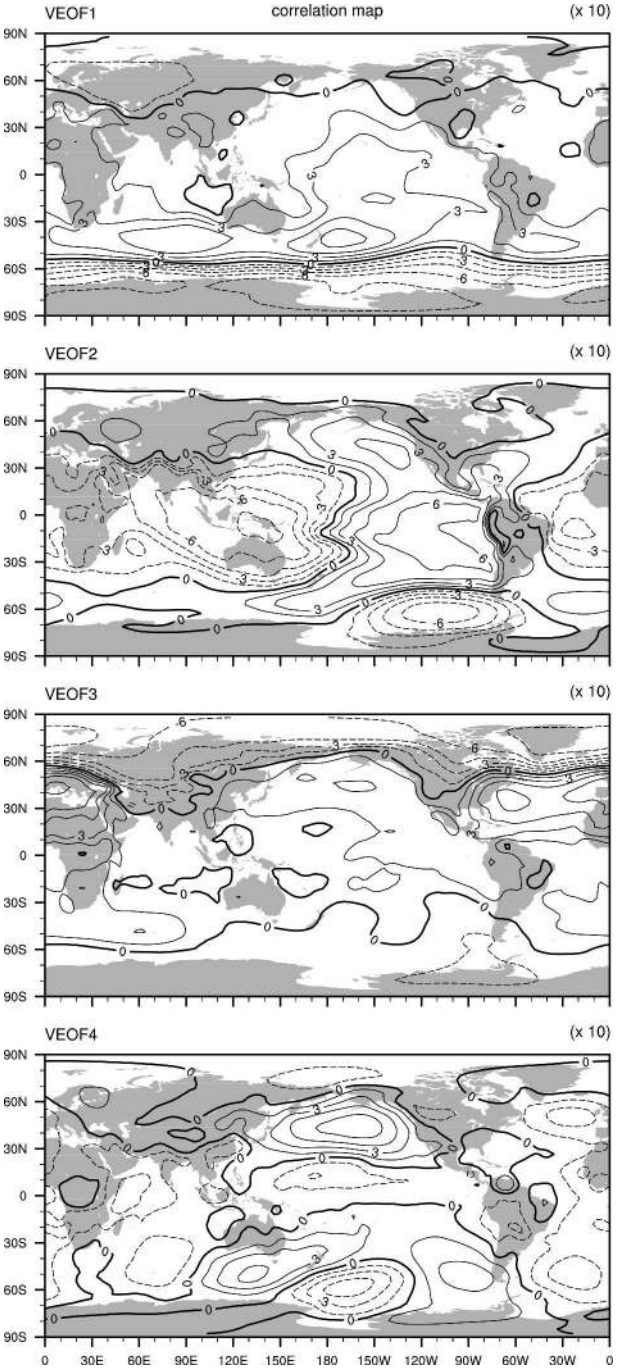

FIG. 5. Correlation patterns corresponding to the first four VEOFs. The contour interval is 0.15, contours are multiplied by 10, and negative values are dashed.

c. Cyclostationary EOFs

We performed CSEOF analyses of the fields with and without the annual cycle included, and the first CSEOF mode with the annual cycle accounted for 46.2% of the variance for unfiltered monthly data and

59.8% of the 1–2–1-filtered data. The patterns of the first mode match the monthly departures from the annual mean. However, when the CSEOF analysis is applied to anomalies, the mean annual cycle is no longer evident, suggesting that the conventional and easiest way to deal with this nonstationary component of the annual cycle is simply to remove the long-term monthly mean annual cycle. We present results for the first two CSEOF mass anomaly modes, which account for 10.5% and 7.8% of the variance, respectively, while the next mode accounts for 5.8% of the variance.

Not unexpectedly, the first pattern that emerges is strongly related to ENSO. The annual cycle of patterns every second month (Fig. 6) reveals similarity to VEOF2 and the strong presence of the SO. Seasonal regressions of sea level pressure with the SOI were given by Trenberth and Caron (2000, their Fig. 4), and the patterns are basically replicated in CSEOF1, indicating the value of the simple SOI based on Tahiti and Darwin pressures alone. In January the deep low pressure in the North Pacific associated with El Niño is dominant and this continues into March, but the wave train in the Southern Hemisphere and the couplet across the South Pacific dominates the rest of the year. Hence this is the pattern that is phase locked to the annual cycle. The correlation of the time series with a low-pass-filtered Niño-3.4 SST index (less than 2 yr fluctuations eliminated; see Fig. 6) is 0.89. The exceptional character of the 1982–83 and 1997–98 events is less evident in the CSEOF series, showing that those events have somewhat different character than the norm, while the weak Pacific warming in 1979 shows up as strongly as the 1976–77 event.

The second CSEOF mode (Fig. 7) appears to map quite well onto the NAO and NAM in the northern winter. Moreover, a low-pass-filtered series that removes fluctuations with < 24 months is correlated with the CSEOF2 at 0.61 for NAO and 0.73 for NAM, suggesting that it is the northern winter variance that dominates. This is confirmed if we correlate only the time series for the six winter and summer months separately. For the NAO with CSEOF2 the correlations using monthly data are 0.36 (0.75) for November to April versus 0.03 (0.10) for May to October, where the values in parentheses are for the 6-month averages; while for NAM the values are 0.46 (0.76) and 0.17 (0.33), respectively. However, in the southern winter, the CSEOF2 pattern has a resemblance to SAM, and correlations with SAM are 0.66 over all months, not varying much from summer to winter, when low-pass filtered. Consequently, CSEOF2 is also correlated 0.50 (low pass) with VEOF1.

Because there is no variance in the CSEOF time series on less than 24-month time scales, only the low-pass-filtered correlations are meaningful. Given that we have 44 years of data and 22 samples of two-yearly values, correlations less than 0.44 are not significant. It seems therefore that there is distinctive phase locking of variance with the annual cycle. However, while the monthly SAM and NAM indices are not significantly correlated at only 0.06, for low-pass data they are correlated 0.31. Hence they separately account for 54% (NAM) and 43% (SAM) of the variance of CSEOF2 of which only 10% of the variance is joint. Thus the CSEOF procedure is combining the essentially separate northern and southern variability into a single mode and can evidently do so because of the relatively few degrees of freedom.

4. Conclusions

In this paper, we have

- exploited the new reanalyses ERA-40 for the 44 years from 1958 to 2001 to provide a new perspective on atmospheric variability at the surface. However, it was necessary to correct for a high bias in surface pressures over the southern oceans prior to 1979 (the corrected dataset is available online at http://www.cgd.ucar.edu/cas/catalog/ecmwf/era40).
- analyzed the global *mass* field for the first time. We suggest that this variable is more physically based than either sea level or surface pressure as the global mean mass for dry air is conserved. The effect is to place more weight on lower-latitude variations relative to sea level pressure analyses.
- analyzed all seasons combined as, globally, winter in one hemisphere is combined with summer in the other hemisphere.
- utilized varimax rotation and clarified the terminology and widespread mislabeling of procedures previously used in atmospheric science in this regard, and further clarified the utility and shortcomings of the varimax rotation.
- developed new software and applied it to cyclostationary analysis of the mass field, with a commentary on its utility and shortcomings (the software is available online at http://www.cgd.ucar.edu/cas/software/list.html).
- related the new results to previous analyses and thereby provided a more rigorous justification for patterns or "modes" of variability that have previously been identified in regional and seasonal analysis. In particular, ENSO, SAM, NAM, the NAO, and NPI emerge as the dominant patterns. We believe that the results for SAM are more reliable than pre-

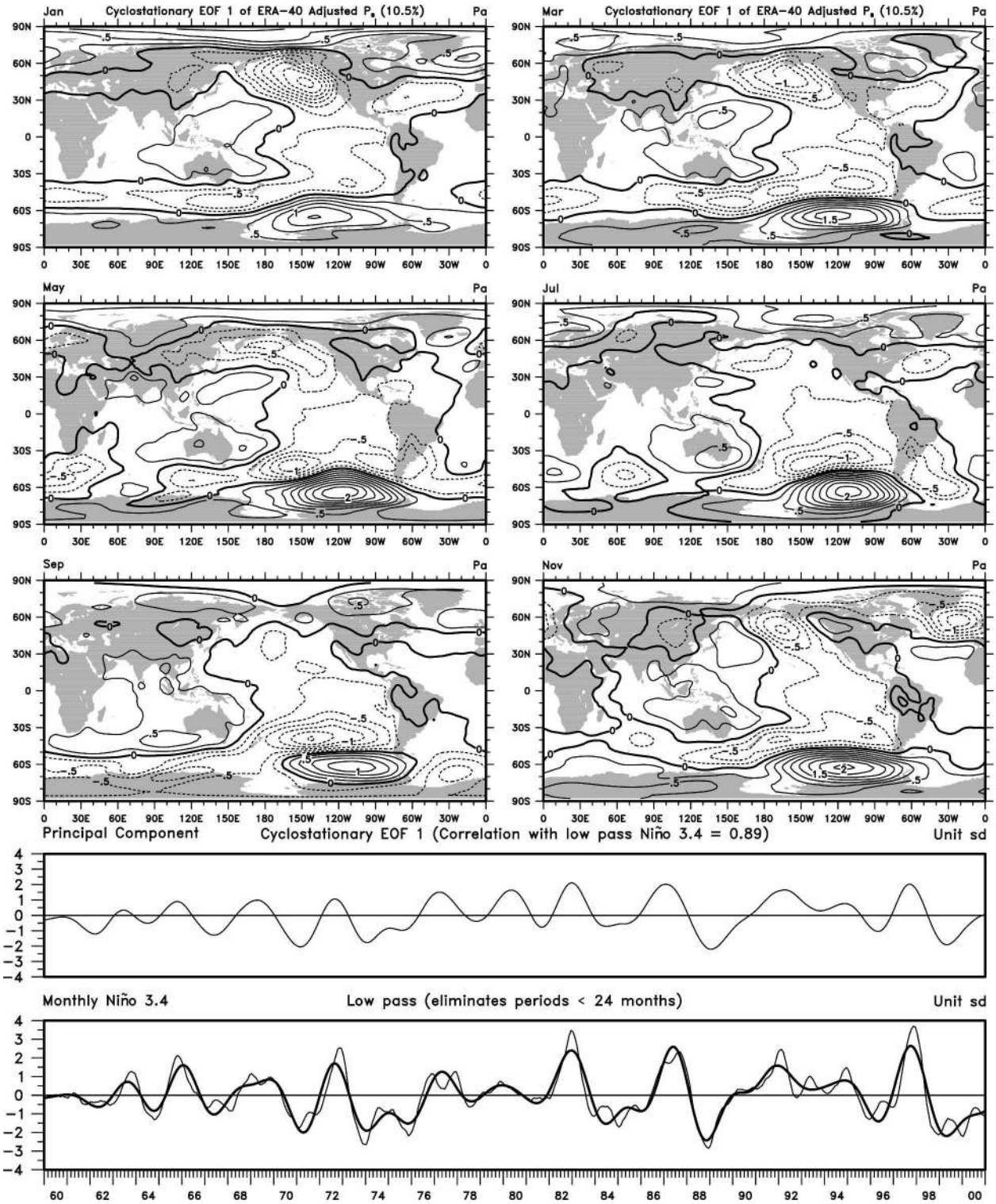

FIG. 6. CSEOF1, which accounts for 10.5% of the variance, is shown with its annual cycle of patterns for every two months of surface pressure anomalies for Jan, Mar, May, Jul, Sep, and Nov, and whose normalized time series is given below. Also shown below is the Niño-3.4-SST index and a smoothed version to eliminate periods less than 24 months (and hence more compatible with frequencies retained by CSEOF1), correlation 0.89.

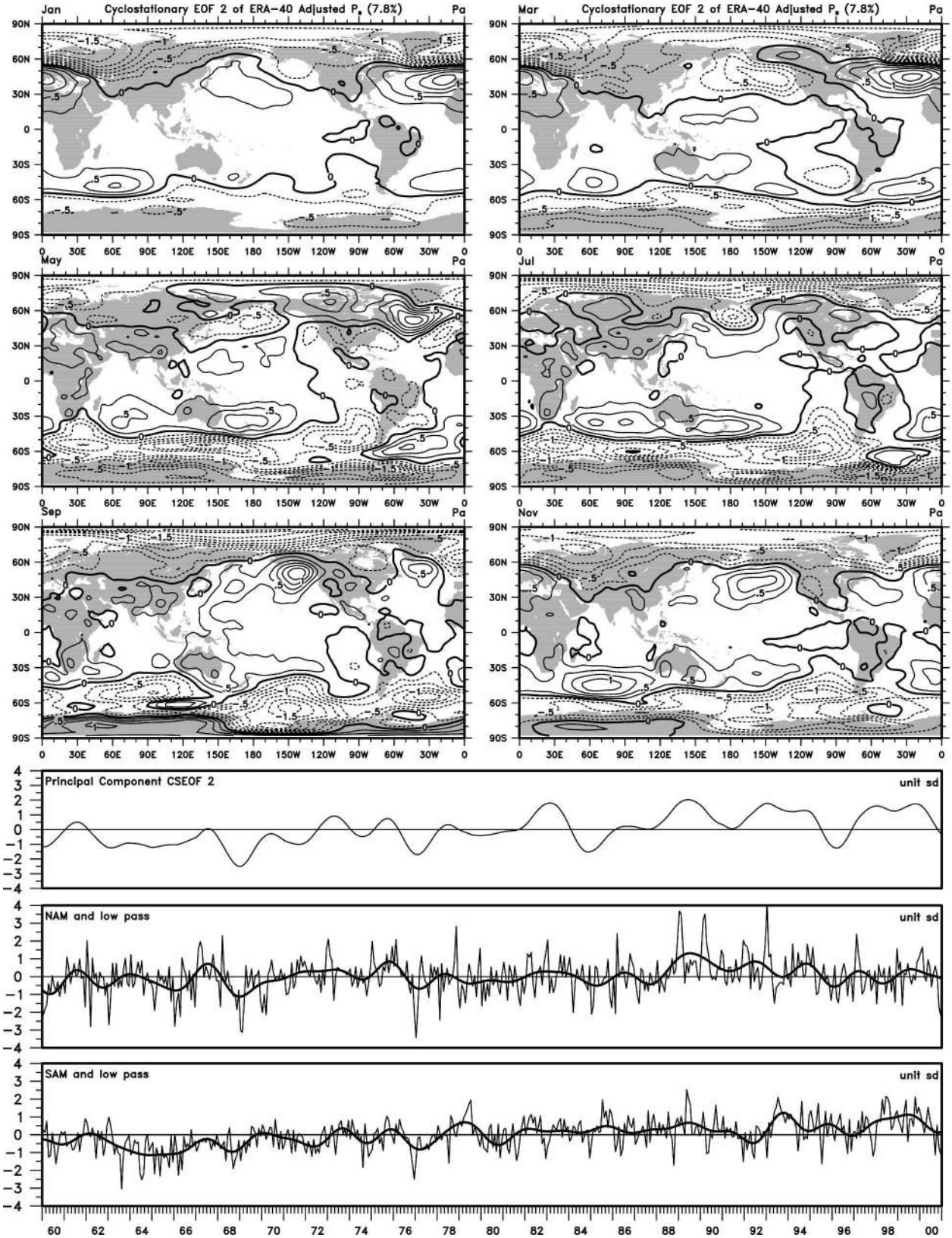

FIG. 7. CSEOF2 (which accounts for 7.8% of the variance) annual cycle of patterns for every two months of ssurface pressure anomalies for Jan, Mar, May, Jul, Sep, and Nov. The normalized time series is given below along with monthly and smoothed series of NAM (correlation 0.73) and SAM (correlation 0.66).

vious analyses owing to problems in analyses over the Southern Hemisphere.
- justified the use of hemispheric analysis for some patterns.

To elaborate further, we argue that owing to the physical constraint of conservation of mass, there is considerable merit in analyzing the atmospheric variability using mass as a variable, rather than surface or sea level pressure; the difference is an area-weighting factor that emphasizes the lower latitudes. Moreover, it applies to any grid without having to worry about convergence of meridians. Nevertheless, we displayed results in the form of equivalent surface pressure anomalies, as they are more familiar. These anomalies should also be more directly related to atmospheric circulation than sea level pressure, which adds an artificial temperature-dependent atmospheric component, but they should also be very similar as the main difference is a bias that does not affect the anomalies much.

In this paper we also use a global domain to capitalize on the constraint, and this means that seasons are opposite in each hemisphere. Seasonality is stronger in the Northern Hemisphere where winter variance is much greater and thus tends to dominate. This approach makes most sense for truly global modes of variability such as ENSO, and the conclusion follows naturally from the results. We first cut down on weather noise that is large in monthly data by smoothing anomalies with the 1–2–1 binomial smoother. We performed a standard EOF analysis of mass based on the covariance matrix, which is therefore an analysis of mass anomalies. Results suggest that this technique convolves true modes of variability, as has been found before. We then explored *R*-mode varimax rotation, which is not a panacea either. However, rotation of four EOFs produced very useful results, with patterns that can be matched to known modes of behavior. Nevertheless, the VEOF patterns are fixed throughout the year. Accordingly, we also performed a cyclostationary EOF analysis, which relaxes the latter constraint and permits the patterns to evolve with the annual cycle. However, it also tends to recover some of the problems with conventional EOF analysis of having mixed modes. Thus it is only the first mode, related to ENSO, that emerges as a useful result from the CSEOF technique. Nevertheless, the results provide useful insights and suggest that employing the technique to more regional domains may be beneficial.

The CSEOF results bring out the patterns that are phase locked to the annual cycle. They have the considerable advantage of allowing the patterns to evolve throughout the year. However, the time series are then restricted to variations greater than 2 yr. CSEOF1 highlights the annual cycle of surface pressure patterns associated with ENSO. It also illustrates that it can deal only with the canonical ENSO and not the multitude of different "flavors" that occur in nature. In particular, the strong 1982/83 and 1997/98 events are not well depicted by this mode. Therefore this example illustrates both the strengths and weaknesses of the method.

CSEOF2 is an interesting pattern but appears to be a mix of hemispheric modes, namely mostly NAM and SAM, that dominate at different times of the year. It seems highly likely that the patterns will depend on the exact period analyzed, and it would take a very long time series before the independence of the two modes is truly revealed, if then (given that climate change makes results nonstationary). Indeed, they may not be independent on decadal time scales owing to common influences on both, such as changes in tropical SSTs (e.g., Hoerling et al. 2001).

The varimax rotation has produced results that align nicely with previously identified patterns of behavior, but the patterns do not evolve with the annual cycle. Accordingly, it is often desirable to analyze the variability by season, as has been common practice in atmospheric science, while recognizing that such a procedure will discriminate against truly global modes of variability. Several studies (Trenberth 1986; Carrera and Gyakum 2003) illustrate this for blocking events, and it is clear that several patterns are needed to describe ENSO, depending particularly on the time of year.

The results provide a rationale for focusing on the NAM, SAM, and ENSO, and with the fourth pattern related to the North Pacific index that in turn is linked to the PDO. Nevertheless, Pacific variability features patterns of decadal SST variability similar to those for ENSO, so it is not independent. The VEOF4 features strong wave train patterns in the Southern Hemisphere as well as the North Pacific center of action, and this also suggests that the Tropics may be involved, but this aspect also likely requires stratification by season to bring further clarification.

The dominant global mode of variability overall is revealed to be one associated with SAM, which is active in all months of the year. It is not very coherent from month to month and appears to exhibit a great deal of natural unforced variability [see Lorenz and Hartmann (2001) for a more complete review of the theory and modeling of SAM]. The third most important mode is NAM and the associated NAO, which is the equivalent Northern Hemisphere expression, as emphasized by Thompson and Wallace (2000), for instance. For

monthly data, ENSO comes in as the second mode, and it is global in extent. However, it also exhibits more coherent evolution with time and projects strongest onto the interannual variability where it stands out as the dominant mode in the CSEOF analysis. As shown, it is coherent with Niño-3.4 SSTs and thus is a coupled mode. This analysis establishes these modes and their ranked importance in more rigorous ways than has been done in the past.

Acknowledgments. This research is partially sponsored by the NOAA CLIVAR and CCDD programs under Grant NA17GP1376. The data used were provided by ECMWF. We thank Dr. K.-Y. Kim for providing the CSEOF software and his help regarding its use, A. Phillips for providing NAO values, and D. Shea for assistance on varimax rotation.

REFERENCES

Barnston, A. O., and R. E. Livezey, 1987: Classification, seasonality and persistence of low-frequency atmospheric circulation patterns. *Mon. Wea. Rev.,* **115,** 1083–1126.

Carrera, M. L., and J. R. Gyakum, 2003: Significant events of interhemispheric atmospheric mass exchange: Composite structure and evolution. *J. Climate,* **16,** 4061–4078.

Davis, J. C., 1986: *Statistics and Data Analysis in Geology*. 2d ed. John Wiley & Sons, 646 pp.

Hoerling, M. P., J. W. Hurrell, and T. Xu, 2001: Tropical origins for recent North Atlantic climate change. *Science,* **292,** 90–92.

Horel, J. D., 1981: A rotated principal component analysis of the interannual variability of the Northern Hemisphere 500 mb height field. *Mon. Wea. Rev.,* **109,** 2080–2092.

Hurrell, J. W., 1995: Decadal trends in the North Atlantic Oscillation: Regional temperatures and precipitation. *Science,* **269,** 676–679.

——, Y. Kushnir, G. Ottersen, and M. Visbeck, 2003: An overview of the North Atlantic Oscillation. *The North Atlantic Oscillation: Climatic Significance and Environmental Impact, Geophys. Monogr.,* No. 134, Amer. Geophys. Union, 1–36.

Jolliffe, I. T., 1987: Rotation of principal components: Some comments. *J. Climatol.,* **7,** 507–510.

Kim, K.-Y., and G. R. North, 1997: EOFs of harmonizable cyclostationary processes. *J. Atmos. Sci.,* **54,** 2416–2427.

——, and C. Chung, 2001: On the evolution of the annual cycle in the tropical Pacific. *J. Climate,* **14,** 991–994.

Lanzante, J. R., 1984: A rotated eigenanalysis of the correlation between 700 mb heights and sea surface temperatures in the Pacific and Atlantic. *Mon. Wea. Rev.,* **112,** 2270–2280.

Lorenz, D. J., and D. L. Hartmann, 2001: Eddy–zonal flow feedback in the Southern Hemisphere. *J. Atmos. Sci.,* **58,** 3312–3327.

Marshall, G. J., 2003: Trends in the southern annular mode from observations and reanalyses. *J. Climate,* **16,** 4134–4143.

Newman, M., G. P. Compo, and M. A. Alexander, 2003: ENSO-forced variability of the Pacific decadal oscillation. *J. Climate,* **16,** 3853–3857.

Richman, M. B., 1986: Rotation of principal components. *J. Climatol.,* **6,** 293–335.

Thompson, D. W. J., and J. M. Wallace, 2000: Annular modes in the extratropical circulation. Part I: Month-to-month variability. *J. Climate,* **13,** 1000–1016.

Trenberth, K. E., 1984: Signal versus noise in the Southern Oscillation. *Mon. Wea. Rev.,* **112,** 326–332.

——, 1986: The signature of a blocking episode on the general circulation in the Southern Hemisphere. *J. Atmos. Sci.,* **43,** 2061–2069.

——, and D. A. Paolino, 1981: Characteristic patterns of variability of sea level pressure in the Northern Hemisphere. *Mon. Wea. Rev.,* **109,** 1169–1189.

——, and J. W. Hurrell, 1994: Decadal atmosphere–ocean variations in the Pacific. *Climate Dyn.,* **9,** 303–319.

——, and J. M. Caron, 2000: The Southern Oscillation revisited: Sea level pressures, surface temperatures, and precipitation. *J. Climate,* **13,** 4358–4365.

——, and D. P. Stepaniak, 2001: Indices of El Niño evolution. *J. Climate,* **14,** 1697–1701.

——, and L. Smith, 2005: The mass of the atmosphere: A constraint on global analyses. *J. Climate,* **18,** 864–875.

——, G. W. Branstator, D. Karoly, A. Kumar, N.-C. Lau, and C. Ropelewski, 1998: Progress during TOGA in understanding and modeling global teleconnections associated with tropical sea surface temperatures. *J. Geophys. Res.,* **103,** 14 291–14 324.